**FOCUS: HONORING HELMUT SCHWARZ'S ELECTION TO THE NATIONAL ACADEMY OF SCIENCES: RESEARCH ARTICLE**

# Elusive Intermediates in the Breakdown Reactivity Patterns of Prodrug Platinum(IV) Complexes

Davide Corinti,[1] Maria Elisa Crestoni,[1] Simonetta Fornarini,[1] Fortuna Ponte,[2]
Nino Russo,[2] Emilia Sicilia,[2] Elisabetta Gabano,[3] Domenico Osella[3]

[1]Dipartimento di Chimica e Tecnologie del Farmaco, Università di Roma "La Sapienza", P.le A. Moro 5, 00185, Rome, Italy
[2]Department of Chemistry and Chemical Technologies, Università della Calabria, Ponte P. Bucci Cubo 14c, 87036, Arcavacata di Rende, Italy
[3]Dipartimento di Scienze e Innovazione Tecnologica, Università del Piemonte Orientale, Viale T. Michel 11, 15121, Alessandria, Italy
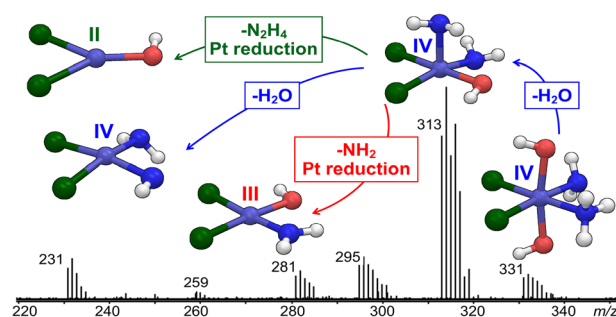
**Abstract.** Kinetically inert platinum(IV) complexes are receiving growing attention as promising candidates in the effort to develop safe and valid alternatives to classical square-planar Pt(II) complexes currently used in antineoplastic therapy. Their antiproliferative activity requires intracellular Pt(IV)–Pt(II) reduction (activation by reduction). In the present work, a set of five Pt(IV) complexes has been assayed using mass spectrometry–based techniques, i.e., collision-induced dissociation (CID), and IR multiple photon dissociation (IRMPD) spectroscopy, together with ab initio theoretical investigations. Breakdown and reduction mechanisms are observed that lead to Pt(II) species. Evidence is found for typically transient Pt(III) intermediates along the dissociation paths of isolated, negatively charged (electron-rich) Pt(IV) prodrug complexes.

**Keywords:** Collision-induced dissociation, IRMPD spectroscopy, FT-ICR mass spectrometry, Reduction processes, Cisplatin
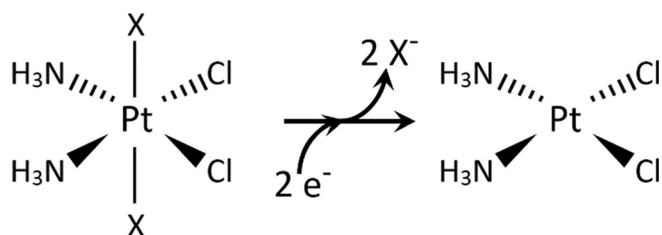
## Introduction

The redox behavior of transition metal complexes has represented an important topic since the dawn of coordination chemistry [1]. In particular, the mechanism of reduction of six-coordinate octahedral $d^6$ Pt(IV) complexes to the corresponding four-coordinate square planar $d^8$ Pt(II) congeners has been intensely studied by Basolo and coworkers [2]. This process

has gained renewed interest since evidence indicated that Pt(IV) anticancer prodrugs are reduced in the hypoxic tumor cells to the pharmacologically active Pt(II) counterparts (Scheme 1) [3–6]. The interpretation of the experimental data concerning such process is not conclusive though [7].

Electrochemical investigations have been hampered by the chemically irreversible character of such a reduction that impedes the evaluation of a meaningful thermodynamic potential [8], as well as by the quick poisoning of the working electrode surface [9]. A number of computational studies at density functional theory (DFT) level have been recently carried out in order to estimate the electrochemical potentials and to suggest a reliable pathway of reduction [10–12]. Interestingly, most of these studies suggested a metastable six-coordinate Pt(III) intermediate. A Pt(III)-containing polymeric material has been indeed described as "platinblau" (platinum blue)

*Correspondence to:* Simonetta Fornarini;
*e-mail:* simonetta.fornarini@uniroma1.it, Emilia Sicilia;
*e-mail:* emilia.sicilia@unical.it, Domenico Osella;
*e-mail:* domenico.osella@uniupo.it

**Scheme 1.** A cisplatin-based Pt(IV) derivative bearing two axial X ligands. The 2e$^-$ reduction produces the active cisplatin metabolite with loss of two X$^-$ anions

because of its characteristic dark blue color. Thus, Pt(III) does exist at least in solid state [13].

Several kinetic experiments on the reduction of Pt(IV) derivatives have been carried out using biological reductants such as ascorbic acid (H$_2$Asc, or more properly at physiologic pH its mono-anion HAsc$^-$), glutathione, cysteine, or methionine [14]. Depending on the kind of the six ligands around the Pt(IV) core and on the nature of the reducing agent, inner-sphere (attack of the reductant especially on hydroxido or chlorido ligands) or outer-sphere redox processes have been suggested [7]. However, it was shown that reduction of Pt(IV) derivatives is mainly carried out by high molecular weight cellular components [15], and Arnesano et al. [16] proved that cytochrome c is indeed able to promote such activation by reduction. Although this mechanism is not fully elucidated in its intimate details, QSAR studies [17] indicated that appropriate reduction potential and lipophilicity are the key factors for designing efficient Pt(IV) anticancer prodrugs. Thus, it is clearly a challenge to ascertain the role of the ligands around the Pt(IV) core and to design new prodrugs with better pharmacokinetics performances.

In view of this highly active interest, a study has been undertaken on possible pathways for the transformation from six-coordinate Pt(IV) to four-coordinate Pt(II) complexes following the evolution of ions sampled by electrospray ionization mass spectrometry (ESI-MS) in negative (deprotonated species) mode. In particular, in the fragmentation scheme of negative ions (electron-rich species, potentially prone to undergo reduction), evidence for intermediates (in particular species formally containing Pt(III)) that are quite elusive in solution [18, 19] is specifically searched, also taking advantage of the long-lived conditions that may be attained by a naked ion in the gas phase. Clearly, this study refers to ionic species isolated in the gas phase rather than to solvated ions or neutrals stabilized by non-covalent interactions in a dielectric medium. It will therefore definitely not provide any direct connection with reaction dynamics in solution or, even less, in vivo. ESI-MS-based methods have been already largely exploited, allowing in-depth studies on the gas phase chemistry of platinum(II) complexes and enabling the determination of ligand binding energies through the measurement of energy-resolved collision-induced dissociation (CID) experiments [20]. In another area, ESI-MS combined with kinetic studies has allowed to establish that cationic platinum(II) complexes are catalytically active in H/D exchanges involving benzene [21]. ESI-MS

coupled with density functional theory (DFT) calculations have shown the occurrence of gas-phase carbon–carbon bond forming reactions catalyzed by Pt(II) and other group 10 metal complexes [22]. Positively charged cisplatin adducts with primary and secondary alcohols have shown C–H bond activation and unexpected dissociation pathways when activated in a linear ion trap [23]. More recently, kinetic and mechanistic features of the ligand exchange reactions of cisplatin-derived aqua complexes have been assayed by ESI coupled with Fourier transform ion cyclotron resonance (FT-ICR) MS [24, 25]. ESI has succeeded in delivering the encounter complexes that play a key role in the ligand displacement reaction in solution, to the gas phase where they have been characterized by both reactivity and spectroscopy [25, 26]. With regard to platinum(IV) complexes, a detailed study has addressed the degradation paths of protonated satraplatin (*trans,cis,cis*-bis(acetato)ammine-cyclohexylaminedichloridoplatinum(IV)), platinum anticancer agent suitable for oral administration [27]. Results based on ESI-MS and DFT calculations have shown that protonation, as verified in the gastric acidic environment, facilitates the loss of the axial ligand, a key step towards the formation of the platinum(II) effective drug. Energy-resolved CID experiments have proven valuable in disclosing the C–C coupling rate-limiting step in alkane reductive elimination from Pt(IV) complexes in the gas phase [28].

While the development of new anticancer drugs has involved the design and synthesis of numerous Pt(IV) compounds [29–32], the present study is focused on a set of compounds characterized by two NH$_3$ molecules in *cis* position in the equatorial plane. Pt(IV) complexes typically display octahedral coordination and react slowly in ligand substitution reactions. The remaining positions in the equatorial plane bear either two chlorido or 1,1-cyclobutanedicarboxylato ligands, and the sampled compounds are shown in Scheme 2. They can be reduced readily to their Pt(II) counterparts, thus behaving as prodrugs, and reactivity can be tuned by the nature of the axial ligands.

High-resolution MS (based on the use of a 7T FT-ICR mass spectrometer in France) and infrared multiple photon dissociation (IRMPD) spectroscopy are employed to gain precise detail on the ion compositions and indication on their structures. The proposed pathways and intermediates are corroborated by means of theoretical calculations at the DFT level.

## Methods

### Sample Preparation

The complexes under investigation, namely (SP-6-33)-diamminedichloridodihydroxidoplatinum(IV) (oxoplatin, EP32, *cis,trans,cis*-PtCl$_2$(OH)$_2$(NH$_3$)$_2$), (SP-6-33)-diacetatodiamminedichloridoplatinum(IV) (EP416, *cis,trans,cis*-PtCl$_2$(CH$_3$COO)$_2$(NH$_3$)$_2$), (SP-6-44)-acetatodiamminedichloridohydroxidoplatinum(IV) (EP417, *cis,trans,cis*-PtCl$_2$(CH$_3$COO)(OH)(NH$_3$)$_2$), (SP-6-33)-diammine(cyclobutane-1,1-dicarboxylato)
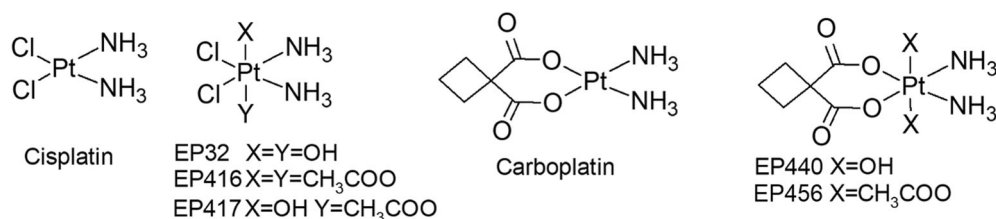
**Scheme 2.** Schematic representation of the sampled Pt(IV) compounds either cisplatin- (EP32, EP416, EP417) or carboplatin-based (EP440, EP456). The structures of the related Pt(II) drugs are also displayed

dihydroxidoplatinum(IV) (EP440, *cis,trans,cis*-Pt$(C_6H_6O_4)(OH)_2(NH_3)_2$), and (SP-6-33)-diacetato-diammine(cyclobutane-1,1-dicarboxylato)platinum(IV) (EP456, *cis,trans,cis*-Pt$(C_6H_6O_4)(CH_3COO)_2(NH_3)_2$), have been prepared according to previously published procedures. In particular, EP32 [17, 33] and EP440 [34] have been synthesized by oxidation of cisplatin or carboplatin with hydrogen peroxide in water.

EP416 [17, 35] and EP456 [36] have been synthesized by the reaction between the corresponding dihydroxido complex and acetic anhydride.

EP417 [37, 38] has been prepared by oxidation of cisplatin with hydrogen peroxide in acetic acid, but the same method has been only partially successful in the case of (SP-6-44)-acetatodiammine(cyclobutane-1,1-dicarboxylato)hydroxidoplatinum(IV), because the synthesis seemed to result in two isomeric products. In fact, HPLC-MS analysis indicated the presence of two chromatographic peaks (in different ratios depending on the reaction time), corresponding to the same MS signal, possibly due to *cis/trans* isomers. The formation of the *cis* isomer has been rarely reported, but it has been already observed for a similar Pt(II) compound containing cyclobutane-1,1-dicarboxylato and 2,2-dimethyl-1,3-propanediamine, in the case of its oxidation with hydrogen peroxide in acetic acid (to *cis*-diacetato Pt(IV) product), with respect to the use of acetic anhydride (*trans*-diacetato Pt(IV) product) [39, 40]. Because the two isomers could not be easily separated and might have different reduction behavior, the (SP-6-44)-acetatodiammine(cyclobutane-1,1-dicarboxylato)hydroxidoplatinum(IV) derivative has been excluded from the present investigation.

All the complexes employed have been washed several times with cold water, methanol, and diethyl ether, and their purity has been checked with HPLC-MS and elemental analysis (within ± 0.4% of the calculated value) as reported elsewhere [41, 42]. This point is particularly important because impurities might give rise to undesired mass signals (above all, when they are easily ionized).

The samples for ESI-MS experiments have been prepared starting from stock solutions of the selected complexes $10^{-3}$ M in water. The solutions have been subsequently diluted in MeOH/$H_2O$ (1:1 *v/v*) to $5 \times 10^{-5}$ M to be directly infused in the ESI source of the MS platforms described in the following section. In order to enhance the abundance of the deprotonated species, an ammonia solution 0.1 M in aqueous methanol has been used as a solvent system.

## Mass Analysis and CID Experiments

Three different mass spectrometry platforms have been employed.

Preliminary MS analyses were conducted in a Paul ion-trap (Esquire 6000, Bruker) through direct infusion of the solutions, prepared as stated above, in the ESI source at a flow rate of 180 μL h$^{-1}$. Typical parameters were a capillary voltage at 3.8 kV and drying gas ($N_2$) fluxed at 7 L/min$^{-1}$ at 300 °C. Soft conditions were needed to avoid unwanted dissociation of the complexes in the ESI process. Therefore, low voltage settings have been used for the capillary exit and the skimmer, respectively, − 60 V and − 45 V. CID experiments have been performed on mass-selected ions using an activation amplitude comprised between 0.20 V and 0.35 V and an activation time of 0.50 ms.

High-resolution mass spectra have been recorded on a hybrid FT-ICR tandem MS (APEX-Qe Bruker Daltonics) sited at the Université Paris-Sud, Orsay. The samples have been directly infused in the ESI source of the mass spectrometer whose capillary voltage has been set to ca. 4 kV. The instrument comprises a quadrupole-hexapole interface to mass select and accumulate ions before the FT-ICR analyzer, equipped with 7.0 T actively shielded cryomagnet. In particular, the Pt(IV) complexes have been mass-selected in the quadrupole and subsequently accumulated for 1 s in the hexapole pressurized with argon. Finally, the ions have been mass-analyzed in a broadband mode using a 2-M data set. Mass spectra result from the accumulation of 30 scans. The elemental composition has been determined comparing the experimentally obtained accurate masses with the exact ones calculated using the isotope list of the National Institute of Standards and Technology (https://physics.nist.gov/cgi-bin/Compositions/stand_alone.pl). The ions have been assigned to their chemical formula with a tolerance below 3 ppm. Accurate masses of the fragments generated by CID of deprotonated EP32, EP416, and EP417 have been also recorded, by performing a mass selection of the precursor ion in the quadrupole sector of the instrument and activation in the hexapole. The accurate masses have been compared with the calculated ones, as previously

described, to assess the chemical composition of the product ions of interest.

CID experiments varying the collision energy (CE) have been carried out using a hybrid triple quadrupole linear ion trap (Q1q2Q$_{LIT}$) instrument (Applied Biosystems API 2000 Q-Trap). The presence of a quadrupole linear ion trap (Q$_{LIT}$) as the third sector of the instrument permits to accumulate the fragments obtained by CID in the second sector (q2) and to increase sensitivity and resolution. The MS parameters used for the experiments are the following: curtain gas at 50.0 psi, ion source gas at 20.0 psi, declustering potential at 30 V, and entrance potential at 5 V. Nitrogen has been used as collision gas at a nominal pressure of $2.7 \times 10^{-5}$ mbar.

### IRMPD Experiments

IR multiple photon dissociation (IRMPD) spectra have been obtained in the 3000–3700 cm$^{-1}$ range (pertinent to X–H (X = C, N, O) stretching modes) employing an optical parametric oscillator/amplifier (OPO/OPA) laser system (LaserVision) pumped by a 10-Hz Nd:YAG laser coupled with a Paul ion-trap (Bruker Esquire 6000) mass spectrometer. The apparatus has been already described in detail [43]. The mass-selected ions have been trapped for 10–40 ms, depending on their abundance, and irradiated for 1 s or 2 s, depending on their ease to undergo fragmentation. The typical output energy from the OPO/OPA laser was 15 mJ pulse$^{-1}$ with a spectral width of 5 cm$^{-1}$. In a few instances, IRMPD has been assisted by a continuous wave CO$_2$ laser [44]. A train of CO$_2$ pulses at 25 Hz has been generated and synchronized with the tunable laser to enhance the fragmentation yield. The CO$_2$ laser pulse length was adjusted so as to avoid IRMPD by the CO$_2$ laser radiation alone. The IR action spectra are obtained by plotting the photofragmentation yield $R = - \ln[I_p/(I_p + \Sigma I_f)]$, where $I_p$ and $\Sigma I_f$ are the parent and sum of the fragment ion intensities, respectively, as a function of the radiation wavenumber [45].

### Computational Details

Geometry optimizations have been performed with the Gaussian09 software package [46], at DFT level using the hybrid Becke three parameter exchange functional [47] and the Lee-Yang-Parr correlation functional [48], B3LYP. To describe the Pt atom, the relativistic compact Stuttgart/Dresden effective core potential [49] in combination with the split valence basis set has been employed. For the rest of the atoms, the standard triple-$\zeta$ quality 6-311++G** basis sets of Pople have been used. Calculation of vibrational frequencies at the same level of theory has been performed to both establish the nature of intercepted stationary points as minima and transition states and get zero point energy (ZPE) corrections. Enthalpies and Gibbs free energies have been obtained at 298 K at 1 atm from total energies, including zero-point and thermal corrections, using standard statistical procedures [50]. The involved transition states have been carefully checked to be properly connected to the correct minima by IRC (intrinsic reaction coordinate) analysis [51, 52].

## Results and Discussion

### Breakdown Behavior of Prodrug Pt(IV) Complexes

The mass spectra of the selected set of compounds, recorded by ESI in negative ion mode, display the pattern of ionic species formed in solution. Common features as well as distinctive trends are observed, depending on individual structures. The mass spectrum of the prototypical complex in the series, namely EP32, is reported in Figure S1 in the Supplementary Material (SM). The major ion cluster in the spectrum corresponds to the deprotonated species [EP32-H]$^-$, confirming the stability of the complex and its resistance to hydrolysis. The isotopic pattern reflects the natural abundances of Pt and Cl isotopes giving rise to the distribution well identified in high-resolution FT-ICR MS. The insert in Figure S1 shows the isotopic cluster while the exact mass measurements on the individual peaks confirm the expected elemental composition. Henceforth, anionic complexes will be associated to and named after the $m/z$ value of the first significant ion in the isotopic cluster. For example, [EP32-H]$^-$ is represented by $m/z$ 331, corresponding to the [{$^{194}$Pt(OH)$_2$($^{35}$Cl)$_2$(NH$_3$)$_2$}-H]$^-$ isotopic composition. Other ions appearing in the mass spectrum are related to [EP32-H-H$_2$O]$^-$ and [EP32+Cl]$^-$, the former due to H$_2$O loss and the second one to the attachment of chloride, a ubiquitous ion in solution. The mass spectra of the other compounds in the series conform to a similar pattern and are displayed in Figures S2–S5. The minor presence of an ion due to water loss is observed also in the mass spectra of EP417 and EP440, while the only negligible loss of acetic acid is found in the mass spectra of EP416, EP417, and EP456.

The naked negatively charged complexes [EPX-H]$^-$ (X = 32, 416, 417, 440, and 456) have been submitted to collision-induced dissociation (CID) aiming to point out fragmentation products discriminating any tendency towards a reduction in oxidation state and ligation number. In these experiments, the energy released on the activated ion may be varied to provide a relative trend of energy thresholds in dissociation processes. When submitted to CID, [EPX-H]$^-$ ions display a complex scheme of parallel and consecutive fragmentation paths. The first step, common to all species, involves loss of an axial ligand and is typically followed by either a direct cleavage of one of the equatorial ligands or a fragmentation process involving reduction of the remaining ionic species. In the following paragraph, the fragmentation of [EP32-H]$^-$ is described in detail and used as a reference for the behavior of other sampled Pt(IV) complexes.

Figure 1 shows the CID mass spectra of selected [EP32-H]$^-$ ions recorded at high resolution in FT-ICR MS. The analogous CID experiments performed on [EPX-H]$^-$ (X = 416, 417, 440) are illustrated in Figures S6–S8 in the SM. Mass spectra are collected in the FT-ICR cell after CID in the quadrupole sector of the instrument run at two different values of collision energy (CE, in the laboratory frame). The main fragment formed from [EP32-H]$^-$ at low CE (4 V) is the product ion at $m/z$ 313 due to loss of water.
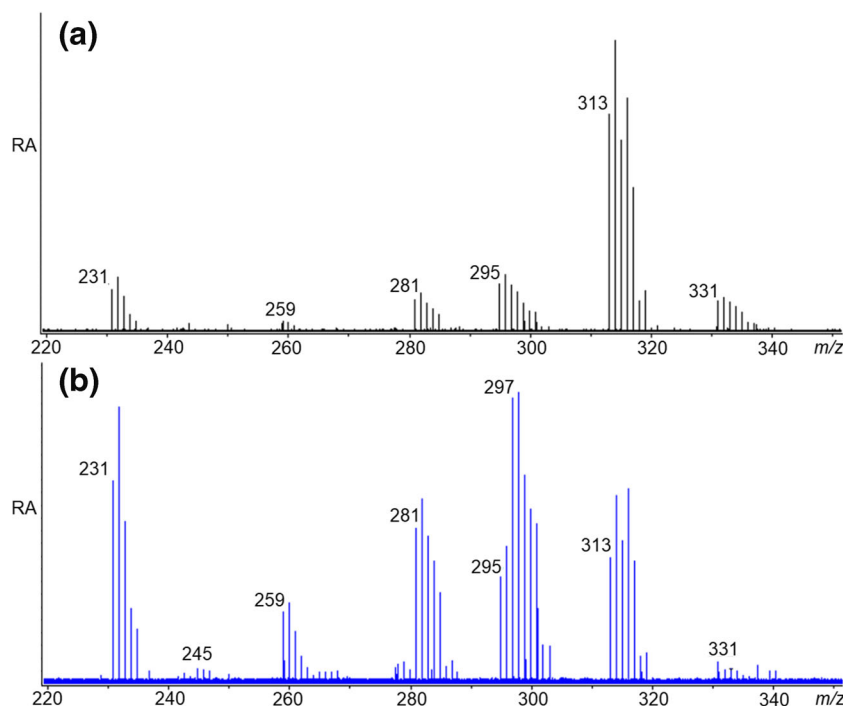
**Figure 1.** CID mass spectrum of [EP32-H]⁻ (*m/z* 331–337) recorded with a collision energy of 4 V (panel (**a**), black profile) and 8 V (panel (**b**), blue profile). Relative abundances (RAs) are in arbitrary units

Increasing the collision energy to 8 V, the abundance of the precursor ion [EP32-H]⁻ at *m/z* 331 becomes negligible and also the relative fraction of [EP32-H-$H_2O$]⁻ at *m/z* 313 decreases in favor of lower mass ions. A complete fragmentation scheme linking all the observed species is obtained by $MS^n$ experiments, in which each individual product ion from [EP32-H]⁻ is submitted to activation and subsequent mass analysis.

The complete frame linking the observed fragments is summarized in Scheme 3, showing that all lower mass fragments are generated from the ion *m/z* 313. As also shown by the CID mass spectrum of [EP32-H]⁻ at 4 V (Figure 1), two main product ions are formed by the subsequent fragmentation of [EP32-H-$H_2O$]⁻ at *m/z* 313, namely an ion at *m/z* 295 corresponding to loss of a second water molecule and an ion at *m/z* 281 involving a neutral loss of 32 Da, possibly accounted for by either NHOH or $N_2H_4$ as neutral fragment. The former possibility involves a single-electron reduction, leading to a formal Pt(III)–containing species, while in the second one, a 2-electron redox process yields a Pt(II) complex [PtCl₂(OH)]⁻. Other fragments also observed in Figure 1 pertain to dissociation paths from the ion at *m/z* 295. In particular, the species at *m/z* 259 derives from HCl loss yielding in turn the ion at *m/z* 231 by loss of $N_2$. Moving to higher CE (Figure 1b), a novel feature regards the formation of an ion at *m/z* 297 with an isotopic cluster overlaying the ion at *m/z* 295. This dissociation channel involves a 16-Da loss that can be ascribed to either $NH_2$ loss, concomitant with a one-electron reduction of the complex, or an O atom loss implying a two-electron reduction.

In order to solve the ambiguities regarding fragments at *m/z* 297 and 281, their accurate mass obtained by high-resolution

(HR) FT-ICR mass spectrometry has been compared with the calculated exact mass for potential candidates. An example of these measurements is provided in Figure 2, an enlargement of the HR mass spectrum of Figure 1b showing that four elemental compositions are contributing to *m/z* 297.

The most abundant peak at *m/z* 296.92210 is assigned to [¹⁹⁴Pt³⁵Cl₂(NH₂)(OH)]⁻ with a confidence of 0.8 ppm, thus confirming the presence of a formal Pt(III)–containing complex generated by a neutral $NH_2$ loss from the *m/z* 313 ion (as displayed in Scheme 3). No signal complying with the elemental composition of a candidate Pt(II) complex [PtCl₂(NH₂)(NH₃)]⁻ has been found, while the *m/z* signals at 296.92734 and 296.93257 are consistent with the presence of the ions [¹⁹⁴Pt³⁵Cl³⁷Cl(NH₂)(NH)]⁻ and [¹⁹⁶Pt³⁵Cl₂(NH₂)(NH)]⁻, respectively, which are part of the isotopic cluster of the fragment generated by water loss from the complex at *m/z* 313. Finally, the ion *m/z* 296.91630 conforms to the formula [¹⁹⁵Pt³⁵Cl₂(NH)(OH)]⁻ arguably obtained from a tiny fraction of secondary $NH_3$ loss (not reported in Scheme 3 due to negligible intensity). The whole set of fragments reported in Scheme 3 has been confirmed comparing the high-resolution experimental mass with the calculated exact mass (Table S2), also assessing the nature of the ion at *m/z* 281, which has been assigned to a formal Pt(II)–containing complex, [PtCl₂(OH)]⁻, generated by $N_2H_4$ loss from [PtCl₂(NH₂)₂(OH)]⁻.

The same procedure has been employed to establish breakdown schemes for [EP416-H]⁻, [EP417-H]⁻, [EP440-H]⁻, and [EP456-H]⁻ (Schemes S1–S4 and Tables S3–S5 in the SM). The schemes display increasing complexity. For example, the dissociation pattern of [EP416-H]⁻ (Scheme S1) entails the
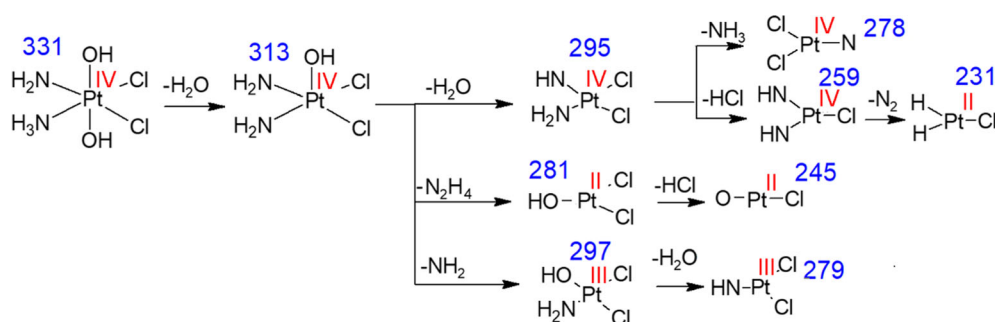
**Scheme 3.** Schematic representation of the dissociation pattern generated by CID of [EP32-H]⁻. The *m/z* ratio of each species is indicated in blue and the formal oxidation state of platinum in red. Every complex is negatively charged; charges are not made explicit

presence of more than 25 different product ions. For the sake of simplicity, we will refer to the primary channels generated from the precursor ion, noting two dissociation paths related to the axial ligands, acetic acid loss and $CH_2COO$ loss, and two fragmentations involving the equatorial ligands, loss of ammonia, and $NH_2Cl$ loss. Interestingly, loss of $CH_2COO$ has been already observed in the degradation of polynuclear platinum complexes bearing acetato ligands, and this fragment has been ascribed to oxacyclopropanone [53]. In this study, a formal Pt(III) dinuclear cluster has been obtained in the gas phase by degradation of a tetrameric compound in the ESI source [53]. The $CH_2COO$ loss channel leads to the formation of a Pt(II) complex, $[PtCl_2(NH_3)_2(CH_3CO_2)]^-$, presenting the base structure of cisplatin with an additional acetato ligand, likely placed in an external coordination sphere [10]. It represents the only dissociation channel involving a redox reaction associated with cleavage of an axial ligand in the whole set of examined Pt(IV) species. The dissociation path involving $NH_2Cl$ loss also requires a redox step generating a Pt(II) complex in which the two axial ligands are still bound to platinum. In contrast, the redox process in water is considered to involve mainly the axial ligands [3, 7, 54, 55], while leaving the equatorial ones untouched. However, a few evidences are reported supporting possible participation of the equatorial ligands in some redox process [30], rather in line with the gas-phase reaction where the equatorial ligands are acting in the reduction reaction of platinum(IV).

In the endeavor to provide a comprehensive description of the breakdown behavior of the sampled complexes, Figure 3 summarizes the normalized intensities of the major dissociation channels of [EPX-H]⁻ (X = 32, 416, 417, 440, 456) at a common CE value.

The behavior of [EP416-H]⁻, compared with that of [EP32-H]⁻, shows less extensive dissociation and the contribution of an important ammonia loss. Moving to [EP417-H]⁻, possessing different axial ligands, the behavior under CID condition reflects its mixed nature showing an intermediate extent of precursor ion fragmentation to yield fragments pertaining to both [EP32-H]⁻ and [EP416-H]⁻, as reported in Scheme 4 (and more thoroughly illustrated in Scheme S2 of the SM). However, the primary water loss is the most prominent

channel (Figure 3), confirming it to be the easiest dissociation path.

Concerning [EP440-H]⁻, it presents the same hydroxido axial ligands as EP32 but differs for the equatorial ligands, where the two chlorido are substituted by a chelating 1,1-cyclobutanedicarboxylato ligand. The low percentage of intact precursor ion makes it similar to [EP32-H]⁻ suggesting the crucial factor that eases the water loss path to be the presence of two hydroxido ligands in axial positions. In addition, one may note the presence of a small fraction of anionic ligand, 1,1-cyclobutanedicarboxylate, dissociating from the complex. Scheme S3 in the SI displays the
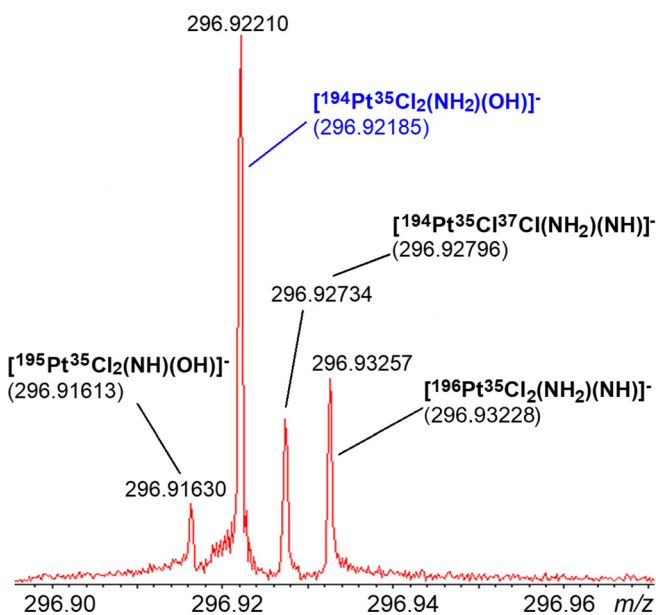


**Figure 2.** Excerpt of the CID mass spectrum of [EP32-H]⁻. The assigned elemental composition is reported for each ion together with the corresponding calculated exact mass in Da (in brackets). The ion corresponding to the Pt(III)-containing complex (in blue) is the most abundant species, while all other species are formal Pt(IV) complexes. Table S1 in the SM provides a comprehensive list of experimental and calculated *m/z* values and associated error
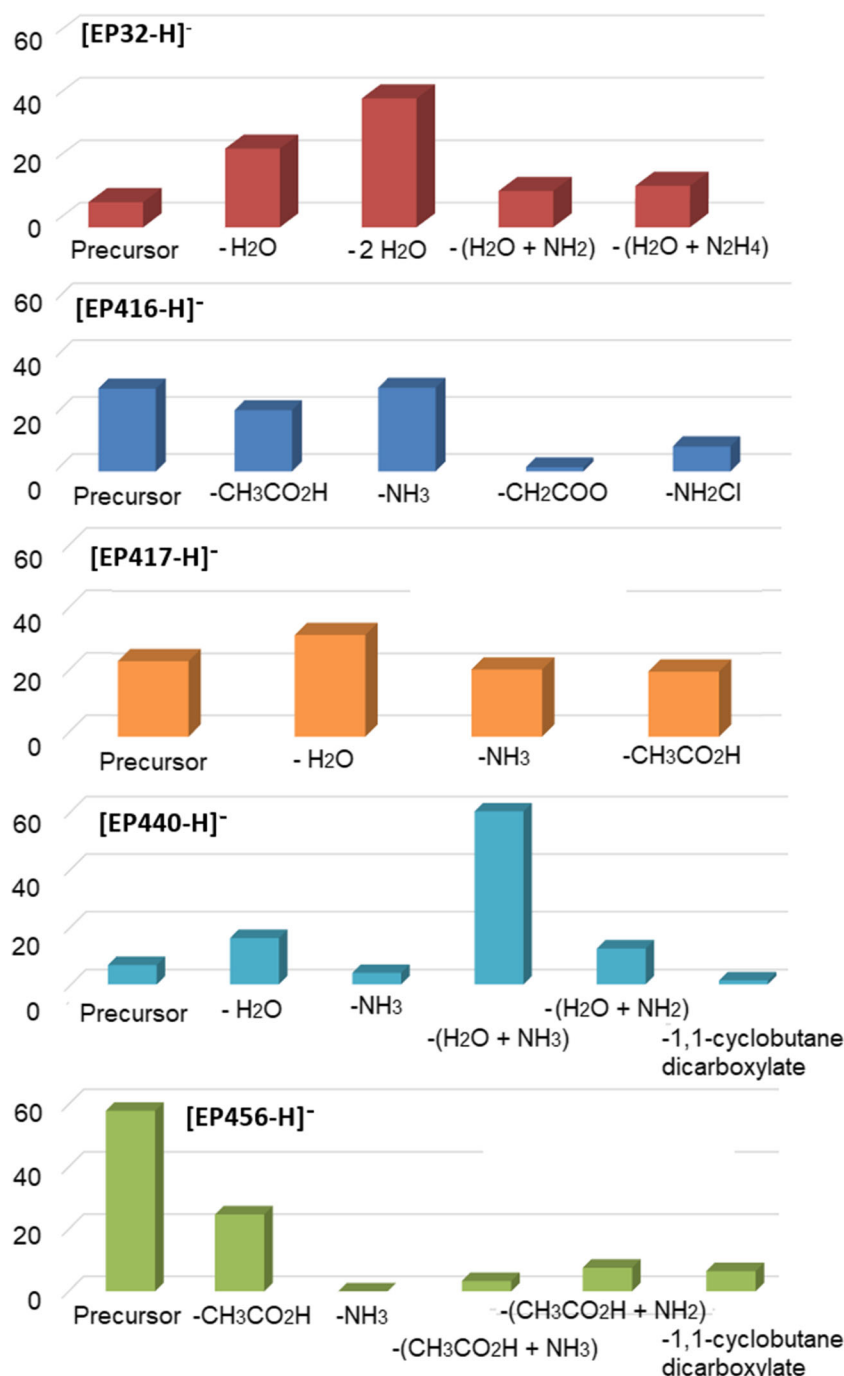
**Figure 3.** Major breakdown channels from deprotonated EPX (X = 32, 416, 417, 440, 456) and their normalized ratio in the CID mass spectrum at CE = 5 V

complete fragmentation pattern of [EP440-H]⁻ showing the presence of a channel producing a formal Pt(III)–containing complex by loss of $NH_2$ following the primary dissociation of water. This channel is instead missing in the CID of [EP416-H]⁻ suggesting the hydroxido ligand to have a major role in the reaction mechanism along the EP32/EP416/EP417 series. The process is conceivably bound to the possibility for the OH to swap from axial to equatorial position, thus replacing the $NH_2$ group in the pentacoordinated complexes formed by the primary water

loss, as further illustrated in the following section. This evidence is limited to the cisplatin prodrugs EP32/EP416/EP417 though. In fact, in the case of EP456, the fragmentation pattern of the deprotonated species, reported in Scheme 5 and, more comprehensively, in Scheme S4, shows the formation of an ion corresponding to [Pt(1,1-cyclobutanedicarboxylato)($CH_3COO$)($NH_2$)]⁻ formally containing Pt(III) despite the absence of any OH ligand. Interestingly, this is also the major secondary channel as shown in Figure 3.
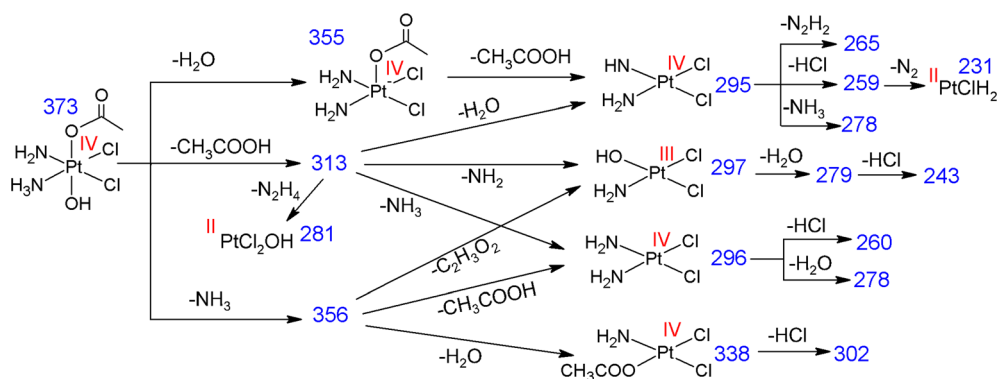
**Scheme 4.** Schematic representation of the dissociation pattern generated by CID of [EP417-H]⁻. The *m/z* ratio of each species is indicated in blue and the formal oxidation state of platinum in red. Every complex is negatively charged; charges are not made explicit

The [Pt(1,1-cyclobutanedicarboxylato)(CH₃COO)(NH₂)]⁻ complex at *m/z* 411 fragments once again by loss of NH₂ forming a Pt(II) complex. This two-step sequence, corresponding to a stepwise reduction from Pt(IV) to Pt(II), is characteristic of EP456 and unusual with respect to the otherwise prevailing direct dissociation of N₂H₄. The [EP456-H]⁻ complex is also the most resistant towards fragmentation, as demonstrated by the high fraction of intact parent ion reported in Figure 3. In this respect, EP456 conforms to the already mentioned lower ease to undergo dissociation shown by complexes presenting two acetato ligands in axial positions.

### Structural Assay of Selected Deprotonated Complexes by IRMPD Spectroscopy

Two species in the set of deprotonated complexes have been selected for an assay by vibrational spectroscopy in the X–H (X = C, N, O) stretching range, namely [EP32-H]⁻ and [EP417-H]⁻, in order to gain direct, experimental evidence on the structure of these species which may be ascertained by comparing experimental IRMPD features with IR spectra of computed structures.

The experimental spectrum of [EP32-H]⁻ in the 3000–3700 cm⁻¹ region is reported in Figure 4 together with the calculated IR spectra for two candidate isomers, EP32_1 and EP32_2.

The first species is obtained from EP32 neutral complex by abstraction of a proton from one of the ammine ligands. This isomer is lower in energy. The search for a local minimum corresponding to deprotonation from the OH group has failed in spite of sustained effort. In the second isomer, EP32_2, a proton has moved from NH₃ to one of the hydroxido ligands. The ensuing species is higher in free energy by 10.0 kcal mol⁻¹. It is thus not surprising that the comparison between experimental and theoretical spectra points to EP32_1 as the major species representing the gas-phase population. The IRMPD spectrum is dominated by a broad and asymmetric feature around 3400 cm⁻¹ comprising two signals at 3410 and 3332 cm⁻¹ (see gray profile in Figure 4 and Table S6 in the SM) which may be ascribed to the asymmetric stretching modes of the intact ammine ligand calculated at 3440 and 3394 cm⁻¹. The sharp feature at 3625 cm⁻¹ can be assigned to the OH stretching mode that is calculated at 3670 cm⁻¹ for EP32_1. Thus, in the experimental spectrum, the OH stretching mode is shifted to a lower value with respect to the calculated
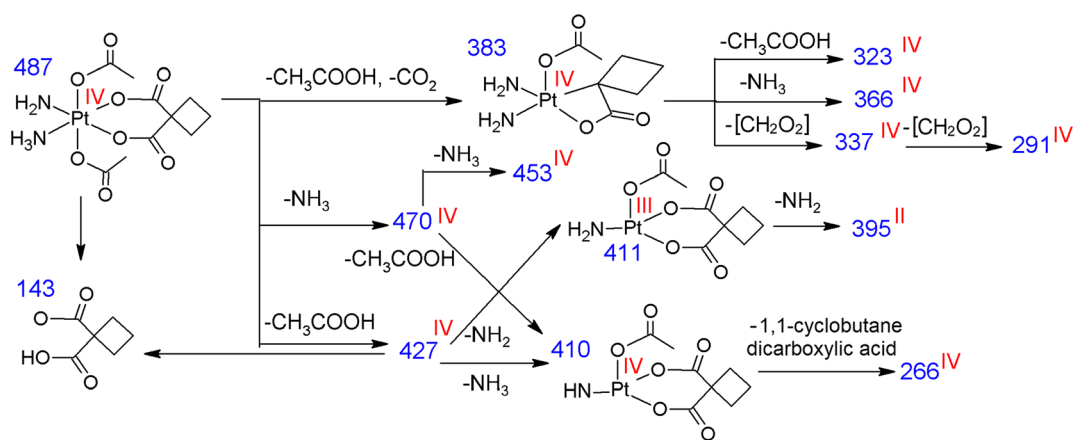
**Scheme 5.** Schematic representation of the dissociation pattern generated by CID of [EP456-H]⁻. The *m/z* ratio of each species is indicated in blue and the formal oxidation state of platinum in red. Every complex is negatively charged; charges are not made explicit
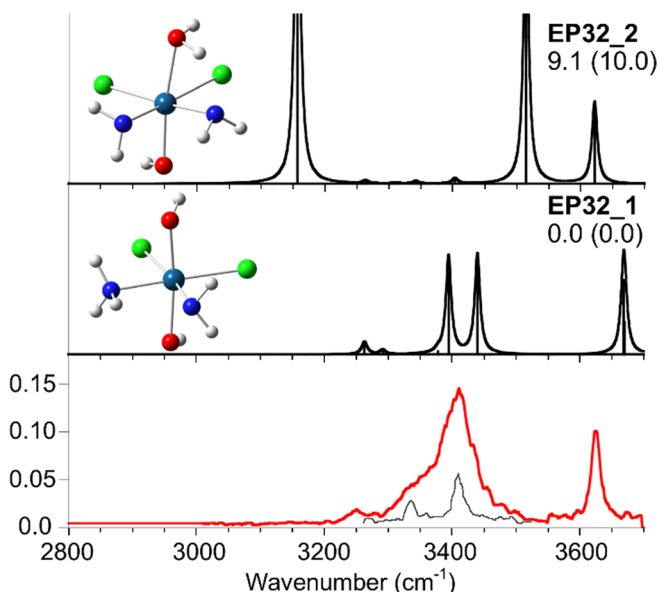
**Figure 4.** IRMPD spectrum of [EP32-H]⁻ (red profile and gray profile recorded at lower laser power) compared with calculated IR spectra for EP32_1 and EP32_2 (black profiles). Optimized geometries are reported together with relative enthalpies and free energies (in brackets) at 298 K in kcal mol¹. A factor of 0.957 is used to scale the calculated harmonic frequencies

IR frequency. This kind of discrepancy is, however, a common finding for the OH stretching mode in related platinum complexes assayed by IRMPD spectroscopy [25]. A small band around 3247 cm$^{-1}$ in the IRMPD spectrum can be assigned to the N–H symmetric stretching calculated at 3263 cm$^{-1}$ for the $NH_3$ ligand in EP32_1. The contribution of EP32_2 to the sampled gas-phase population is unlikely, in view of the absence of any IRMPD activity in the 3500–3550 and 3100–3200 cm$^{-1}$ ranges. In fact, isomer EP32_2 is expected to present strong absorptions near 3515 and 3158 cm$^{-1}$, related to the $H_2O$ asymmetric and symmetric stretching modes,
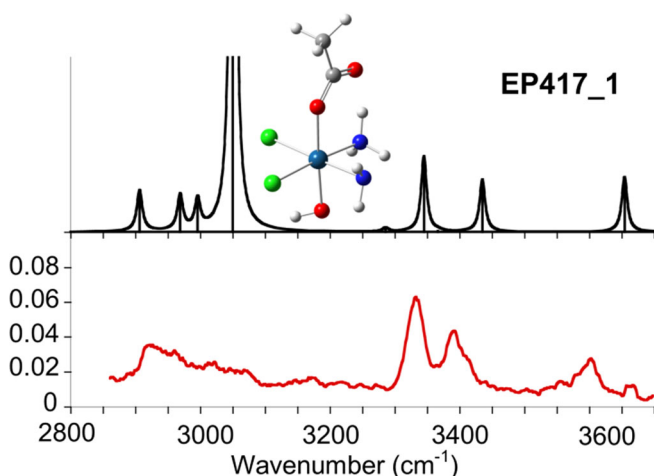


**Figure 5.** IRMPD spectrum of [EP417-H]⁻ (red profile) compared with the IR spectrum of EP417_1 (black profile). The optimized geometry is reported. A factor of 0.957 is used to scale the calculated harmonic frequencies

respectively. Their relatively low wavenumber in the calculated spectrum is due to the interaction of the water hydrogen atoms with nitrogen of equatorial $NH_2$. This isomer is rather likely to play a role as intermediate in the water loss path, the largely prevailing dissociation process in the breakdown chemistry of [EP32-H]⁻.

IRMPD spectroscopy has also been used to inquire about the structural and vibrational features of [EP417-H]⁻. Figure 5 shows the experimental spectrum (red profile) to be compared with the IR spectrum (black profile) for the optimized geometry of the lowest lying conformer of [EP417-H]⁻, namely EP417_1. Once again, the deprotonation site is an ammine ligand. No other isomers have been found exploring possible prototropic rearrangements. A few other conformers of EP417_1 have been also considered, involving modifications in the Pt-O-C angle and rotations around the O-Pt-O axis. The optimized geometries and their relative enthalpies and free energies are reported in Figure S9 together with their calculated IR spectra. However, the presence of these higher lying conformers in the sampled gas-phase population is unlikely on the basis of both their high relative free energy compared to the global minimum ($G_{rel}$(298 K) ≥ 6.4 kcal mol$^{-1}$) and the comparison of calculated and experimental spectroscopic features. We will therefore refer to the lowest lying conformer EP417_1 in discussing the experimental IR features.

The IRMPD spectrum (Figure 5 and Table S7) shows a signal at 3605 cm$^{-1}$, matching the OH stretching frequency calculated at 3654 cm$^{-1}$ [25], which is followed by two features at 3397 and 3330 cm$^{-1}$ fairly well accounted for by the $NH_3$ asymmetric stretching modes calculated at 3435 and 3345 cm$^{-1}$. In the spectral range below 3100 cm$^{-1}$, one may recognize a broad asymmetric absorption with maximum around 2920 cm$^{-1}$ that can be attributed to a combination of the asymmetric and symmetric stretching modes of the methyl group (2996, 2969, and 2906 cm$^{-1}$, respectively) with the symmetric stretching of ammonia at 3050 cm$^{-1}$. This latter vibrational mode is red-shifted due to H-bonding between a positively polarized hydrogen of $NH_3$ oriented towards the carbonyl oxygen of the acetato ligand. This stabilizing interaction undoubtedly contributes to this geometry being the lowest lying in energy. It also explains the low activity of the experimental feature and its broad width, as extensively reported in the literature [56–59].

## Computed Paths for the Gas-Phase Breakdown Pattern

DFT calculations have been employed to outline the free energy profile for the gas-phase fragmentation pattern of two sampled Pt(IV) complexes. Figure 6 presents the potential energy surface (PES) for the [EP32-H]⁻ complex. IRMPD evidence has pointed to the EP32_1 structure for [EP32-H]⁻ involving deprotonation at an ammine ligand.

Water loss is the common first event, prior to subsequent dissociation steps as depicted in Scheme 3. The water loss process in the dissociation pathway of [EP32-H]⁻ occurs in two steps, namely proton transfer from the remaining $NH_3$
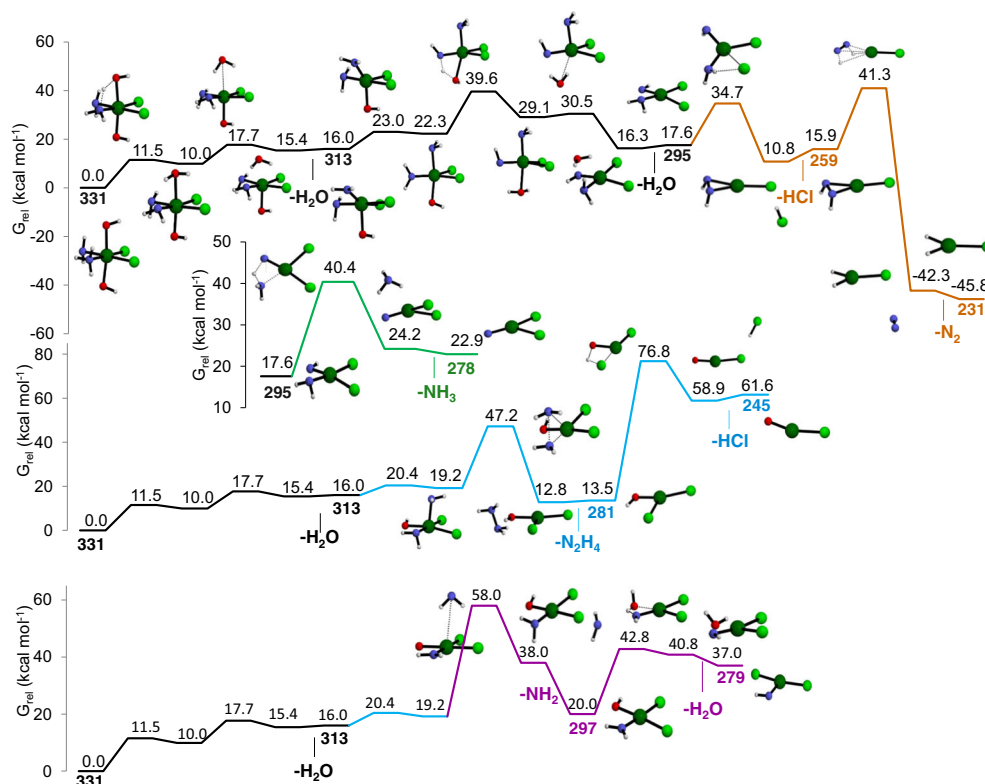
**Figure 6.** PES for the breakdown pattern of [EP32-H]$^-$. The black trace, common to all profiles, regards the common water loss process. The neutral losses for all dissociation paths are indicated below the colored lines. Relative free energies at 298 K in kcal mol$^{-1}$ are reported in black. The $m/z$ value for each species is reported in color

ligand within EP32_1 to an axial OH (forming EP32_2) and detachment of the so-formed water molecule. The two corresponding intercepted transition states lie at 11.5 and 17.7 kcal mol$^{-1}$ for the former and the latter step, respectively. These relatively low values are in agreement with the observed ease for fragmentation even at low CE (Figures 1a and 3). The overall process for dissociation of water from [EP32-H]$^-$ yielding the product ion at $m/z$ 313 results to involve a $\Delta G$ value of 16.0 kcal mol$^{-1}$. Subsequent fragmentation paths entail competing losses of a second H$_2$O molecule, N$_2$H$_4$, and NH$_2$. For the second water loss, it is necessary to overcome three transition states involving motion of one of the NH$_2$ groups from equatorial to axial position, transfer of one hydrogen from the NH$_2$ group in equatorial position to OH, and detachment of the so-formed water. The three transition states lie at 23.0, 39.6, and 30.5 kcal mol$^{-1}$, respectively (black profile, Figure 6). For N$_2$H$_4$ and NH$_2$ release, the corresponding transitions states lie at 47.2 (blue profile, Figure 6) and 58.0 (purple profile, Figure 6) kcal mol$^{-1}$, respectively. The data are consistent with the behavior of [EP32-H]$^-$ which shows a preferential second-step fragmentation involving water loss ($m/z$ 295) and loss of N$_2$H$_4$ ($m/z$ 281) at 4 V CE (Figure 1a). At this CE value, hardly any product involving NH$_2$ loss is formed while it becomes a prevailing species at 8 V CE (Figure 1b). At this same CE, the product at $m/z$ 295 undergoes subsequent dissociation yielding ions at $m/z$ 259, $m/z$ 231, and $m/z$ 278. The last one is the least abundant (Figure 1b) in agreement with the higher activation

free energy (40.4 kcal mol$^{-1}$, green profile of Figure 6) compared to the 34.7 kcal mol$^{-1}$ needed to activate the loss of HCl from $m/z$ 295 (orange profile, Figure 6). Finally, the ion $m/z$ 259 generates the fragment at $m/z$ 231 in a process involving N$_2$ loss as shown in Scheme 3. This latter dissociation channel presents a calculated transition state energy of 16.7 kcal mol$^{-1}$, lower than the one involved in the secondary channel involving loss of NH$_2$, as shown in the orange and purple profiles of Figure 6, respectively.

Overall, the computational survey offers a reliable description and interpretation of the experimentally observed phenomena. A few details regarding the reaction mechanism can be underlined, focusing in particular on the processes generating the reduced platinum species. There are three paths leading to either Pt(II) ($m/z$ 231 and 281) or Pt(III) ($m/z$ 297) species that are formed via a redox process involving the former ammonia molecules bound to the metal. Indeed, it is a different landscape when compared with the reactivity pattern in solution where reduction of platinum(IV) is accompanied by oxidation and dissociation of the axial ligands [7, 17, 30, 32]. However, in the naked gaseous platinum(IV) complex, water molecules are largely lost by direct cleavage concomitant with proton transfer from the ammine ligand, whose acidity is enhanced by ligation to the metal. The so-formed *cis* NH$_2$ groups react upon CID by donating two electrons to the electron-poor Pt(IV) atom to generate a N–N bond leading to dissociation (blue profile in Figure 6). In contrast, the reaction producing the Pt(III)
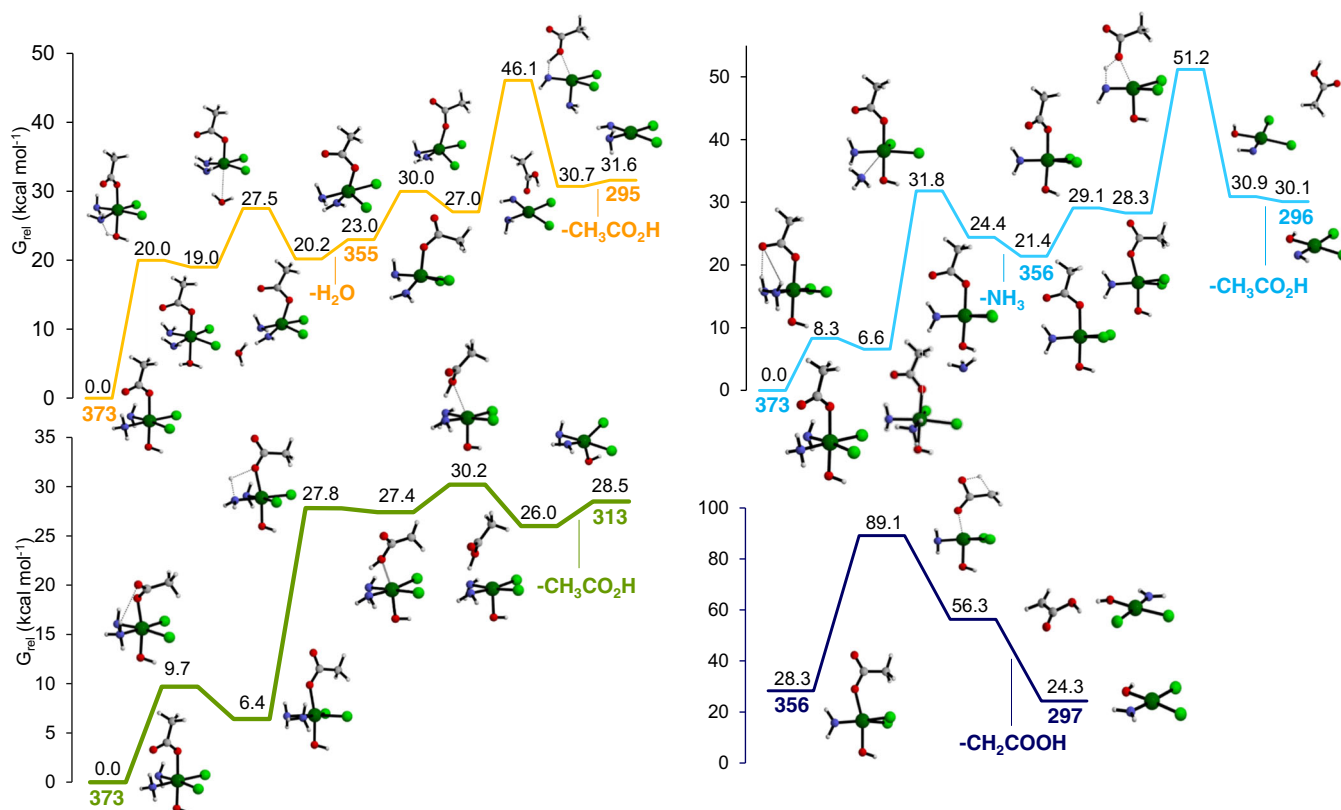
**Figure 7.** PES for the breakdown pattern of [EP417-H]⁻. The neutral losses for all dissociation events are indicated below the colored lines. Relative free energies at 298 K in kcal mol⁻¹ are reported in black. The m/z value for each species is reported in color

complex proceeds by a direct cleavage of NH₂ with a preliminary swapping of the hydroxido axial group to the equatorial position forming a complex where the NH₂ group is in axial position. The so-formed Pt(III) complex [PtCl₂(OH)(NH₂)]⁻ is stable enough and can be isolated and subsequently assayed in the gas phase in spite of there being no clearcut evidence for the formation of Pt(III) species in the reaction paths of Pt(IV) complexes in solution.

The second Pt(IV) complex sampled by DFT calculations is [EP417-H]⁻, where deprotonation has once again interested one of the NH₃ ligands, as shown by the IRMPD spectroscopic assay. The different ligands in the axial position open a larger variety of breakdown paths as reported in Scheme 4 and Scheme S2. The calculated PES for the early steps in the dissociation pattern is depicted in Figure 7 and shows the first competing processes involving loss of either water (orange profile), acetic acid (green profile), or ammonia (pale blue profile). The pathway for water cleavage illustrated in the yellow profile comprises two steps. Starting from the most stable structure, corresponding to EP417_1, the transition state for proton shift from NH₃ to the axial OH group lies at 20.0 kcal mol⁻¹. The subsequent event of H₂O cleavage involves a barrier at 27.5 kcal mol⁻¹. The magnitude of the overall activation barrier for water loss is thus significantly higher than the one affecting the departure of water from EP32_1, which is in agreement with the comparatively limited dissociation of [EP417-H]⁻ relative to [EP32-H]⁻ (Figure 4).

As already noticed, the hydrogen bond between a proton belonging to NH₃ and the carbonyl group of the acetato ligand exerts a stabilizing influence. However, this interaction needs to be released in order to activate the NH₃ cleavage process, which occurs by way of a transition state at 8.3 kcal mol⁻¹ relative to EP417_1 (see pale blue profile in Figure 7) to achieve a higher energy structure at 6.6 kcal mol⁻¹ relative energy (named EP417_3 in the survey of [EP417-H]⁻ geometries collected in Figure S9). EP417_3 then releases NH₃ after passing a barrier at 31.8 kcal mol⁻¹ in an overall 21.4 kcal mol⁻¹ endoergic process. The third possible primary cleavage of [EP417-H]⁻ ions concerns acetic acid loss. Once again, a proton migration event is required which needs a rotational rearrangement of EP417_1 to be activated. As shown in the green profile of Figure 7, EP417_1 isomerizes to a structure (EP417_2 in Figure S9) lying at 6.4 kcal mol⁻¹, whereby the methyl hydrogens are oriented towards the two chlorido ligands. From this configuration, a transition state for proton shift from NH₃ to acetate is reached at 27.8 kcal mol⁻¹, and finally, overcoming a barrier at 30.2 kcal mol⁻¹, acetic acid is released in an overall 28.5 kcal mol⁻¹ endoergic process. One may notice that the highest lying transition state for acetic acid loss (at 30.2 kcal mol⁻¹) is rather close to the one for NH₃ departure (31.8 kcal mol⁻¹). This nearly negligible difference may account for the similar ease for acetic acid vs. NH₃ loss that results from the data displayed in Figure 3.

It may be underlined that also the breakdown pattern of [EP417-H]$^-$ shows the formation of products where the metal has formally undergone reduction. Thus, the ion at $m/z$ 313, corresponding to $[Pt(OH)Cl_2(NH_2)_2]^-$, a common species in the fragmentation landscape of [EP32-H]$^-$, confirms here the reduction to a Pt(II) product, $[Pt(OH)Cl_2]^-$, concomitant with cleavage of $N_2H_4$. Also, the formal Pt(III) complex already observed in the breakdown pattern of [EP32-H]$^-$, $[Pt(OH)Cl_2(NH_2)]^-$, is formed along the pathway depicted in dark blue in Figure 7 involving loss of $CH_2COOH$, an oxidation product of acetic acid. In this case, the reduction is accompanying the cleavage of a former axial ligand, occurring, however, only after the release of $NH_3$. The process is reminiscent of the fragmentation pathway by loss of an acetyloxyl radical from a gaseous uranyl complex, thus undergoing reduction from $U^{VI}O_2^{2+}$ to $U^VO_2^+$ [60]. The formation of reduced species after CID activation has indeed been reported in the breakdown behavior of deprotonated uranyl-containing complexes [61–63], while the corresponding protonated species showed no tendency to undergo reduction reactions [62].

## Conclusions

The ESI-MS study of the breakdown pattern of negatively charged ions corresponding to deprotonated platinum(IV) complexes EPX (X = 32, 416, 417, 440, 456), prodrugs for the widely used cisplatin and carboplatin anticancer agents, has revealed a highly varied landscape, modulated by the nature of the axial ligands as well as by the equatorial ones. The deprotonated, negatively charged ions have been purposely assayed, aiming to verify reduction processes leading to platinum(II) species. To this end, a detailed survey of CID schemes has been accomplished, whereas IRMPD spectroscopy has provided the means to ascertain the structure of the starting sampled ions. The ammine ligand has thus been found to be the preferred deprotonation site. When interrogated by CID, the deprotonated species show a complex dissociation pattern, involving axial ligand as well as ammonia loss and dissociation channels eventually leading to reduction of the metal. Interestingly, the reduction processes observed upon activation towards CID have been always accompanied by equatorial ligand loss, either ammine or chlorido. In contrast, reduction reactions from Pt(IV) complexes in condensed phase are considered to be concomitant with axial ligand loss. In this regard, the reduced species characterized using ESI and high-resolution mass spectrometry present alternative paths in the reduction mechanism of platinum(IV) complexes.

Noteworthyly, the gas-phase activation of [EP32-H]$^-$, [EP417-H]$^-$, [EP440-H]$^-$, and [EP456-H]$^-$ has permitted to isolate and characterize platinum complexes with formal metal oxidation state of +3. Platinum(III)-containing species have been seldom observed in solution and only theoretically postulated in the reaction mechanism of Pt(IV) prodrugs. However, as shown in the present work, the mononuclear Pt(III) complexes generated by dissociation in the gas phase have been found to be stable enough to be isolated and further activated. Finally, DFT calculations on the free energy paths for the observed fragmentation reactions have provided theoretical support for the CID dissociation patterns, viewed in the light of thermodynamic reasons.

As an ending note, one may restate that the observed breakdown reactivity patterns describe high energy paths as available to isolated ionic species activated to undergo CID. However, high-resolution FT-ICR mass spectrometry is highly efficient in uncovering the potentially cytotoxic reactivity properties of platinum(IV) complexes, as comprehensively described in a recent report on light-driven platination of neuropeptides having a role in some types of cancer [5].

## Acknowledgements

## References

1. Taube, H.: Electron Transfer Reactions of Complex Ions in Solution. Academic Press, New York (1970)
2. Basolo, F., Morris, M.L., Pearson, R.G.: Bridged mechanism for the platinum(II) catalysis of chloride exchange in chloroammine-platinum(IV) complexes. Disc. Faraday Soc. **29**, 80–91 (1960)
3. Hall, M.D., Hambley, T.W.: Platinum(IV) antitumour compounds: their bioinorganic chemistry. Coord. Chem. Rev. **232**, 49–67 (2002)
4. Venkatesh, V., Sadler, P.J.: Platinum(IV) prodrugs in metal ions in life sciences, Volume 18. In: Sigel, A., Sigel, H., Freisinger, E., Sigel, R.K.O. (eds.), Metallo-Drugs: Development and Action of Anticancer Agents, pp. 69–108. de Gruyter GmbH, Berlin, DE (2018)
5. Wootton, C.A., Sanchez-Cano, C., Lopez-Clavijo, A.F., Shaili, E., Barrow, M.P., Sadler, P.J., O'Connor, P.B.: Sequence-dependent attack on peptides by photoactivated platinum anticancer complexes. Chem. Sci. **9**, 2733–2739 (2018)
6. Hall, M.D., Mellor, H.R., Callaghan, R., Hambley, T.W.: Basis for design and development of platinum(IV) anticancer complexes. J. Med. Chem. **50**, 3403–3411 (2007)
7. Wexselblatt, E., Gibson, D.: What do we know about the reduction of Pt(IV) pro-drugs? J. Inorg. Biochem. **117**, 220–229 (2012)
8. Platts, J.A., Ermondi, G., Caron, G., Ravera, M., Gabano, E., Gaviglio, L., Pelosi, G., Osella, D.: Molecular and statistical modeling of reduction peak potential and lipophilicity of platinum(IV) complexes. J. Biol. Inorg. Chem. **16**, 361–372 (2011)
9. McCormick, M.C., Schultz, F.A., Baik, M.-H.: Glassy carbon electrodes deliver unpredictable reduction potentials for platinum(IV) antitumor prodrugs. Polyhedron. **103**, 28–34 (2016)
10. McCormick, M.C., Keijzer, K., Polavarapu, A., Schultz, F.A., Baik, M.H.: Understanding intrinsically irreversible, non-nernstian, two-electron redox processes: a combined experimental and computational study of the electrochemical activation of platinum(IV) antitumor prodrugs. J. Am. Chem. Soc. **136**, 8992–9000 (2014)
11. Šebesta, F., Baxová, K., Burda, J.V.: Redox potentials for tetraplatin, satraplatin, its derivatives, and ascorbic acid: a computational study. Inorg. Chem. **57**, 951–962 (2018)

12. Tolbatov, I., Coletti, C., Marrone, A., Re, N.: Insight into the electro-chemical reduction mechanism of Pt(IV) anticancer complexes. Inorg. Chem. 57, 3411–3419 (2018)

13. Gillard, R.D., Wilkinson, G.: Platinum blue and related compounds. J. Chem. Soc. 2835–2837 (1964)

14. Jovanović, S., Petrović, B., Bugarčić, Ž.D., van Eldik, R.: Reduction of some Pt(IV) complexes with biologically important sulfur-donor ligands. Dalt. Trans. 42, 8890–8896 (2013) and references therein

15. Nemirovski, A., Kasherman, Y., Tzaraf, Y., Gibson, D.: Reduction of cis,trans,cis-[PtCl₂(OCOCH₃)₂(NH₃)₂] by aqueous extracts of cancer cells. J. Med. Chem. 50, 5554–5556 (2007)

16. Lasorsa, A., Stuchlíková, O., Brabec, V., Natile, G., Arnesano, F.: Activation of platinum(IV) prodrugs by cytochrome c and characterization of the protein binding sites. Mol. Pharm. 13, 3216–3223 (2016)

17. Gramatica, P., Papa, E., Luini, M., Monti, E., Gariboldi, M.B., Ravera, M., Gabano, E., Gaviglio, L., Osella, D.: Antiproliferative Pt(IV) complexes: synthesis, biological activity, and quantitative structure–activity relationship modeling. J. Biol. Inorg. Chem. 15, 1157–1169 (2010)

18. Ojha, R., Boas, J.F., Deacon, G.B., Junk, P.C., Bond, A.M.: EPR spectroscopic characterization of a monomeric PtᴵᴵᴵI species produced via electrochemical oxidation of the anticancer compound trans-[Ptᴵᴵ{(p-HC₆F₄)NCH₂CH₂NEt₂}cl(Py)]. J. Inorg. Biochem. 162, 194–200 (2016)

19. Rivada-Wheelaghan, O., Ortuño, M.A., García-Garrido, S.E., Díez, J., Alonso, P.J., Lledós, A., Conejero, S.: A stable, mononuclear, cationic Pt(III) complex stabilised by bulky N-heterocyclic carbenes. Chem. Commun. 50, 1299–1301 (2014)

20. Hammad, L.A., Gerdes, G., Chen, P.: Electrospray ionization tandem mass spectrometric determination of ligand binding energies in platinum(II) complexes. Organometallics. 24, 1907–1913 (2005)

21. Gerdes, G., Chen, P.: Cationic platinum(II) carboxylato complexes are competent in catalytic arene C−H activation under mild conditions. Organometallics. 23, 3031–3036 (2004)

22. Woolley, M., Ariafard, A., Khairallah, G.N., Kwan, K.H.-Y., Donnelly, P.S., White, J.M., Canty, A.J., Yates, B.F., O'Hair, R.A.J.: Decarboxylative-coupling of allyl acetate catalyzed by group 10 organometallics, [(Phen)M(CH₃)]⁺. J. Org. Chem. 79, 12056–12069 (2014)

23. Springer, A., Bürgel, C., Böhrsch, V., Mitrić, R., Bonačić-Koutecký, V., Linscheid, M.W.: The gas-phase chemistry of cis-diammineplatinum(II) complexes: a joint experimental and theoretical study. ChemPhysChem. 7, 1779–1785 (2006)

24. Corinti, D., Coletti, C., Re, N., Piccirillo, S., Giampà, M., Crestoni, M.E., Fornarini, S.: Hydrolysis of Cis- and transplatin: structure and reactivity of the aqua complexes in a solvent free environment. RSC Adv. 7, 15877–15884 (2017)

25. Corinti, D., Coletti, C., Re, N., Chiavarino, B., Crestoni, M.E., Fornarini, S.: Cisplatin binding to biological ligands revealed at the encounter complex level by IR action spectroscopy. Chem. Eur. J. 22, 3794–3803 (2016)

26. Corinti, D., Coletti, C., Re, N., Paciotti, R., Maître, P., Chiavarino, B., Crestoni, M.E., Fornarini, S.: Short-lived intermediates (encounter complexes) in cisplatin ligand exchange elucidated by infrared ion spectroscopy. Int. J. Mass Spectrom. 435, 7–17 (2019)

27. Ritacco, I., Al Assy, M., Abd El-Rahman, M.K., Fahmy, S.A., Russo, N., Shoeib, T., Sicilia, E.: Hydrolysis in acidic environment and degradation of satraplatin: a joint experimental and theoretical investigation. Inorg. Chem. 56, 6013–6026 (2017)

28. Couzijn, E.P.A., Kobylianskii, I.J., Moret, M.-E., Chen, P.: Experimental gas-phase thermochemistry for alkane reductive elimination from Pt(IV). Organometallics. 33, 2889–2897 (2014)

29. Johnstone, T.C., Suntharalingam, K., Lippard, S.J.: The next generation of platinum drugs: targeted Pt(II) agents, nanoparticle delivery, and Pt(IV) prodrugs. Chem. Rev. 116, 3436–3486 (2016)

30. Gibson, D.: The mechanism of action of platinum anticancer agents—what do we really know about it? Dalt. Trans. 0, 10681–10689 (2009)

31. Gabano, E., Ravera, M., Osella, D.: Pros and cons of bifunctional platinum(IV) antitumor prodrugs: two are (not always) better than one. Dalt. Trans. 43, 9813–9820 (2014)

32. Petruzzella, E., Sirota, R., Solazzo, I., Gandin, V., Gibson, D.: Triple action Pt(IV) derivatives of cisplatin: a new class of potent anticancer agents that overcome resistance. Chem. Sci. 9, 4299–4307 (2018)

33. Gabano, E., Ravera, M., Trivero, F., Tinello, S., Gallina, A., Zanellato, I., Gariboldi, M.B., Monti, E., Osella, D.: The cisplatin-based Pt(IV)-dichlorofibrato multi-action anticancer prodrug exhibits excellent performances also under hypoxic conditions. Dalt. Trans. 47, 8268–8282 (2018)

34. Varbanov, H.P., Valiahdi, S.M., Kowol, C.R., Jakupec, M.A., Galanski, M., Keppler, B.K.: Novel tetracarboxylatoplatinum(IV) complexes as carboplatin prodrugs. Dalt. Trans. 41, 14404–14415 (2012)

35. Zanellato, I., Bonarrigo, I., Colangelo, D., Gabano, E., Ravera, M., Alessio, M., Osella, D.: Biological activity of a series of cisplatin-based aliphatic bis(carboxylato) Pt(IV) prodrugs: how long the organic chain should be? J. Inorg. Biochem. 140, 219–227 (2014)

36. Giandomenico, C.M., Abrams, M.J., Murrer, B.A., Vollano, J.F., Barnard, C.F.J., Harrap, K.R., Goddard, P.M., Kelland, L.R., Morgan, S.E.: Synthesis and reactions of a new class of orally active Pt(IV) antitumour complexes. In: Howell, S.B. (ed.) Platinum and Other Metal Coordination Compounds in Cancer Chemotherapy, pp. 93–100. Plenum, New York (1991)

37. Ravera, M., Gabano, E., Zanellato, I., Fregonese, F., Pelosi, G., Platts, J.A., Osella, D.: Antiproliferative activity of a series of cisplatin-based Pt(IV)-acetylamido/carboxylato prodrugs. Dalt. Trans. 4, 5300–5309 (2016)

38. Ravera, M., Gabano, E., Tinello, S., Zanellato, I., Osella, D.: May glutamine addiction drive the delivery of antitumor cisplatin-based Pt(IV) prodrugs? J. Inorg. Biochem. 167, 27–35 (2017)

39. Wilson, J.J., Lippard, S.J.: Synthetic methods for the preparation of platinum anticancer complexes. Chem. Rev. 114, 4470–4495 (2014)

40. Lee, Y.-A., Yoo, K.H., Jung, O.-S., et al.: Bull. Chem. Soc. Jpn. 76, 107–110 (2003)

41. Alessio, M., Zanellato, I., Bonarrigo, I., Gabano, E., Ravera, M., Osella, D.: Antiproliferative activity of Pt(IV)-bis(carboxylato) conjugates on malignant pleural mesothelioma cells. J. Inorg. Biochem. 129, 52–57 (2013)

42. Ravera, M., Gabano, E., Pelosi, G., Fregonese, F., Tinello, S., Osella, D.: A new entry to asymmetric platinum(IV) complexes via oxidative chlorination. Inorg. Chem. 53, 9326–9335 (2014)

43. Sinha, R.K., Maître, P., Piccirillo, S., Chiavarino, B., Crestoni, M.E., Fornarini, S.: Cysteine radical cation: a distonic structure probed by gas phase IR spectroscopy. Phys. Chem. Chem. Phys. 12, 9794–9800 (2010)

44. Sinha, R.K., Nicol, E., Steinmetz, V., Maître, P.: Gas phase structure of micro-hydrated [Mn(ClO₄)]⁺ and [Mn₂(ClO₄)₃]⁺ ions probed by infrared spectroscopy. J. Am. Soc. Mass Spectrom. 21, 758–772 (2010)

45. Prell, J.S., O'Brien, J.T., Williams, E.R.: IRPD spectroscopy and ensemble measurements: effects of different data acquisition and analysis methods. J. Am. Soc. Mass Spectrom. 21, 800–809 (2010)

46. Frisch, M.J., Trucks, G.W., Schlegel, H.B., Scuseria, G.E., Robb, M.A., Cheeseman, J.R., Scalmani, G., Barone, V., Mennucci, B., Petersson, G.A., Nakatsuji, H., Caricato, M., Li, X., Hratchian, H.P., Izmaylov, A.F., Bloino, J., Zheng, G., Sonnenberg, J.L., Hada, M., Ehara, M., Toyota, K., Fukuda, R., Hasegawa, J., Ishida, M., Nakajima, T., Honda, Y., Kitao, O., Nakai, H., Vreven, T., Montgomery Jr., J.A., Peralta, J.E., Ogliaro, F., Bearpark, M., Heyd, J.J., Brothers, E., Kudin, K.N., Staroverov, V.N., Keith, T., Kobayashi, R., Normand, J., Raghavachari, K., Rendell, A., Burant, J.C., Iyengar, S.S., Tomasi, J., Cossi, M., Rega, N., Millam, J.M., Klene, M., Knox, J.E., Cross, J.B., Bakken, V., Adamo, C., Jaramillo, J., Gomperts, R., Stratmann, R.E., Yazyev, O., Austin, A.J., Cammi, R., Pomelli, C., Ochterski, J.W., Martin, R.L., Morokuma, K., Zakrzewski, V.G., Voth, G.A., Salvador, P., Dannenberg, J.J., Dapprich, S., Daniels, A.D., Farkas, Ö., Foresman, J.B., Ortiz, J.V., Cioslowski, J., Fox, D.J.: Gaussian 09, revision D.01. Gaussian, Inc., Wallingford (2010)

47. Becke, A.D.: Density-functional thermochemistry. III. The role of exact exchange. J. Chem. Phys. 98, 5648–5652 (1993)

48. Lee, C., Yang, W., Parr, R.G.: Development of the Colle-Salvetti correlation-energy formula into a functional of the electron density. Phys. Rev. B. 37, 785–789 (1988)

49. Andrae, D., Häussermann, U., Dolg, M., Stoll, H., Preuss, H.: Energy-adjusted ab initio pseudopotentials for the second and third row transition elements. Theor. Chim. Acta. 77, 123–141 (1990)

50. McQuarrie, D.A., Simon, J.D.: Molecular Thermodynamics. University Science Books, Sausalito (1999)

51. Fukui, K.: Formulation of the reaction coordinate. J. Phys. Chem. 74, 4161–4163 (1970)

52. Gonzalez, C., Schlegel, H.B.: An improved algorithm for reaction path following. J. Chem. Phys. 90, 2154–2161 (1989)

53. Butschke, B., Schwarz, H.: The "missing link": the gas-phase generation of platinum-methylidyne clusters PtₙCH⁺ (N=1, 2) and their reactions with hydrocarbons and ammonia. Chem. Eur. J. 17, 11761–11772 (2011)

54. Choi, S., Filotto, C., Bisanzo, M., Delaney, S., Lagasee, D., Whitworth, J.L., Jusko, A., Li, C., Wood, N.A., Willingham, J., Schwenker, A., Spaulding, K.: Reduction and anticancer activity of platinum(IV) complexes. Inorg. Chem. **37**, 2500–2504 (1998)

55. Ravera, M., Gabano, E., Zanellato, I., Bonarrigo, I., Escribano, E., Moreno, V., Font-Bardia, M., Calvet, T., Osella, D.: Synthesis, characterization and antiproliferative activity on mesothelioma cell lines of bis(carboxylato)platinum(IV) complexes based on picoplatin. Dalt. Trans. **41**, 3313–3320 (2012)

56. Oomens, J., Steill, J.D., Redlich, B.: Gas-phase IR spectroscopy of deprotonated amino acids. J. Am. Chem. Soc. **131**, 4310–4319 (2009)

57. Roithovà, J.: Characterization of reaction intermediates by ion spectroscopy. Chem. Soc. Rev. **41**, 547–559 (2012)

58. Corinti, D., De Petris, A., Coletti, C., Re, N., Chiavarino, B., Crestoni, M.E., Fornarini, S.: Cisplatin primary complex with L-histidine target revealed by IR multiple photon dissociation (IRMPD) spectroscopy. ChemPhysChem. **18**, 318–325 (2017)

59. Leavitt, C.M., Deblase, A.F., Johnson, C.J., Van Stipdonk, M., McCoy, A.B., Johnson, M.A.: Hiding in plain sight: unmasking the diffuse spectral signatures of the protonated N-terminus in isolated dipeptides cooled in a cryogenic ion trap. J. Phys. Chem. Lett. **4**, 3450–3457 (2013)

60. Perez, E., Hanley, C., Koehler, S., Pestok, J., Polonsky, N., Van Stipdonk, M.: Gas phase reactions of ions derived from anionic uranyl formate and uranyl acetate complexes. J. Am. Soc. Mass Spectrom. **27**, 1989–1998 (2016)

61. Dau, P.D., Gibson, J.K.: Halide abstraction from halogenated acetate ligands by actinyls: a competition between bond breaking and bond making. J. Phys. Chem. A. **119**, 3218–3224 (2015)

62. Van Stipdonk, M.J., Chien, W., Anbalagan, V., Bulleigh, K., Hanna, D., Groenewold, G.S.: Gas-phase complexes containing the uranyl ion and acetone. J. Phys. Chem. A. **108**, 10448–10457 (2004)

63. Van Stipdonk, M., Bubas, A., Tatosian, I., Perez, E., Polonsky, N., Metzler, L., Somogyi, A.: Formation of $[U^{V}OF_4]^-$ by collision-induced dissociation of a $[U^{VI}O_2(O_2)(O_2C\text{-}CF_3)_2]^-$ precursor. Int. J. Mass Spectrom. **424**, 58–64 (2018)